Geoscientific
Model Development

Model description paper

GEMS v1.0: Generalizable Empirical Model of Snow Accumulation and Melt, based on daily snow mass changes in response to climate and topographic drivers

Atabek Umirbekov[1,2,5]**, Richard Essery**[3]**, and Daniel Müller**[1,2,4]

[1]Leibniz Institute of Agricultural Development in Transition Economies (IAMO), Theodor-Lieser-Str. 2,
06120 Halle (Saale), Germany
[2]Geography Department, Humboldt-Universität zu Berlin, Unter den Linden 6, 10099 Berlin, Germany
[3]School of Geosciences, University of Edinburgh, Edinburgh, EH9 3JW, United Kingdom
[4]Integrative Research Institute on Transformations of Human–Environment Systems (IRI THESys),
Humboldt Universität-zu-Berlin, Berlin, Germany
[5]Tashkent Institute of Irrigation and Agricultural Mechanization Engineers (TIIAME),
39 Kari Niyazov Str., Tashkent, 100000, Uzbekistan

Correspondence: Atabek Umirbekov (umirbekov@iamo.de)

Abstract. Snow modelling is often hampered by the availability of input and calibration data, which can affect the choice of models, their complexity, and transferability. To address the trade-off between model parsimony and transferability, we present the Generalizable Empirical Model of Snow Accumulation and Melt (GEMS), a machine-learning-based model, which requires only daily precipitation, temperature or its daily diurnal cycle, and basic topographic features to simulate snow water equivalent (SWE). The model embeds a support vector regression pretrained on a large dataset of daily observations from a diverse set of the SNOw-pack TELemetry Network (SNOTEL) stations in the United States. GEMS does not require any user calibration, except for the option to adjust the temperature threshold for rain–snow partitioning, though the model achieves robust simulation results with the default value. We validated the model with long-term daily observations from numerous independent SNOTEL stations not included in the training and with data from reference stations of the Earth System Model–Snow Model Intercomparison Project. We demonstrate how the model advances large-scale SWE modelling in regions with complex terrain that lack in situ snow mass observations for calibration, such as the Pamir and Andes mountains, by assessing the model's ability to reproduce daily snow cover dynamics. Future model improvements should consider the effects of vegetation, improve simulation accuracy for shallow snow in warm locations at lower elevations, and possibly address wind-induced snow redistribution. Overall, GEMS provides a new approach for snow modelling that can be useful for hydroclimatic research and operational monitoring in regions where in situ snow observations are scarce.

1 Introduction

Snow is a vital component of the global climate system and plays a key role in regulating the temperature of the Earth's surface and in governing the hydrologic cycle on both global and regional scales (Zhang, 2005; Sturm et al., 2017). Furthermore, snow plays an important role as a natural means of water storage and supply for human activities (Barnett et al., 2005), with a substantial share of the world's population relying on snowmelt to provide water for agriculture and domestic needs (Mankin et al., 2015; Kraaijenbrink et al., 2021). Snowmelt is particularly crucial for densely populated downstream areas, where the timing and quantity of snow accumulation and melting in mountainous regions determine the availability of water (Armstrong et al., 2019; Im-

merzeel et al., 2020). Accurate estimation of snow mass accumulation and melt is therefore essential for water resource management, as well as for early warning of droughts and floods (Beniston, 2008).

Energy balance and temperature index snow models are the two main types of models used to simulate snow accumulation and melting. Energy balance snow models, also referred to as physics-based models, calculate the amount of snow mass, based on the balance between the energy input to the snowpack and the energy output from the snowpack (Essery, 2019). These models consider multiple factors such as incoming solar radiation, air temperature, humidity, precipitation, and wind speed, as well as the physical properties of the snowpack, such as snow density and surface albedo. Due to the high input data requirement of energy balance models, which are often lacking especially in countries of the Global South, researchers often opt for relatively simpler conceptual temperature index models, which rely on temperature and precipitation data (Hock, 2003; Ohmura, 2001). These models estimate the amount of snowmelt by determining empirical relationship between temperature and the amount of snowmelt (Link et al., 2019). The two types of snow models usually require an adjustment of the internal parameters that characterize embedded snow processes. Depending on the complexity of a model, calibrating its parameters can often become a computational burden and introduces the challenge of model parameter equifinality (Beven, 1993, 2006; Günther et al., 2020).

Despite the differences in the number of internal processes represented and the corresponding data requirements, both types of models produce similar results when calibrated and applied to the same spatial domain and same climatic conditions (Kumar et al., 2013; Bavera et al., 2014; Magnusson et al., 2011; Shakoor et al., 2018). The growing number of the intercomparison studies conclude that model complexity does not determine performance (Essery et al., 2013; Magnusson et al., 2015; Menard et al., 2021), and simpler models may perform equally well or even outperform more sophisticated snow models in some cases; e.g. when input data are of low quality (Terzago et al., 2020). Models calibrated to the same climate conditions can, however, produce different simulations under different climate conditions (Carletti et al., 2022). In this regard, physics-based snow models are known to show better temporal and spatial transferability than temperature index models (Magnusson et al., 2015), since they are able to capture the dynamic physical processes that govern formation, accumulation, and melting of snow, which allows them to simulate snow under a wide range of climate conditions. The generalizability and transferability of snow models are important considerations in their development and deployment, especially for applications over geographical domains where in situ snow measurements are nonexistent or scarce.

In recent years, the research community saw an emergence of so-called data-driven approaches for snow modelling, which usually employ machine learning techniques on extensive sets of snow observations and predictor variables. In terms of ways in which machine learning (ML) has been applied for snowpack modelling, the respective research studies can be grouped into several main approaches. One common approach is estimating the spatial distribution of snowpack by applying ML-supported interpolation of sparse snow observations and using topographical features and meteorological and satellite data (Broxton et al., 2019; Mital et al., 2022). Other studies have explored the potential of satellite radar data for the direct detection of instantaneous properties of snowpack (Santi et al., 2022; Daudt et al., 2023). In cases where several gridded snow products are available, ML can be employed for a better prediction through the assimilation of multiple estimates or bias correction (Shao et al., 2022; King et al., 2020). A few recent studies applied ML in a manner consistent with traditional snow models, explicitly modelling snow mass accumulation and melt dynamics (Vafakhah et al., 2022; Duan et al., 2023; Wang et al., 2022). However, most of the noted approaches also rely on in situ observations or an extensive set of regional reanalysis variables, which restricts their wider applicability due to unavailability of such data in many regions. Furthermore, the ability of pretrained machine learning models to generalize to new geographic and climatic domains remains another challenge; machine learning models often perform less well outside the data distribution used to train them (Chase et al., 2022; Hernanz et al., 2022).

We address these challenges with the Generalizable Empirical Model of Snow Accumulation and Melt (GEMS) that, by leveraging the power of machine learning to learn from a large number of diverse experiments, generates accurate estimates of snow water equivalent (SWE) from a limited range of input data. Instead of modelling snow as a dynamic system, the GEMS employs assimilated statistical relationship between changes in snow mass in response to climate variables, while accounting for topographic features. By incorporating diverse climate and topographic observations into the model training, we demonstrate how it simulates snow water equivalent with acceptable accuracy even in distant out-of-sample geographical locations.

2 Model description

2.1 Model structure and required inputs

GEMS is an empirical model based on statistical learning of daily changes in snow water equivalent in response to precipitation, temperature, and topography. It incorporates support vector regression (SVR) that was trained using more than 28 000 observations of daily snow accumulation and melt from 94 stations of the SNOwpack TELemetry Network (SNOTEL) in the United States. The model has only one adjustable parameter, namely a temperature threshold (T_S) that

specifies when 100 % of precipitation falls as snow, which is used to confine the SVR simulations during the rain-to-snow transition and snow accumulation phases. Figure 1 depicts the model's workflow and its primary components, which are described in greater detail in the following sections.

The GEMS v1.0 model is developed in the R programming environment (R Core Team, 2020), with anticipated replication in Python and possibly other program languages. It is available as a pretrained SVR model, accompanied by an R script containing a set of functions that take input data on daily time steps, calculate additional predictors, and generate corresponding estimates of snow water equivalent. It can be applied for both single-point and spatially distributed simulations by feeding input data in tabular form or raster files, respectively.

The model is available in four variations in the required input data listed in Table 1. The simplest one, GEMS-4P (the "P" suffix specifies the number of required inputs), requires four predictors, such as daily precipitation, average temperature, latitude, and elevation. Three other modifications, GEMS-5P, GEMS-6P, and GEMS-7P, require additional predictors, such as daily diurnal temperature range (daily maximum and minimum temperatures) and a location-specific heat–insolation index, which can be retrieved through the Google Earth Engine.

2.2 Support vector regression

In its core embedding, GEMS is built on a pretrained SVR that estimates daily accumulation and melt of SWE, given the meteorological conditions and terrain features. SVR is a supervised machine learning algorithm that projects data into a higher-dimensional space and then minimizes the error by generating a set of hyperplanes that explain as many observations as possible (Awad and Khanna, 2015; Vapnik, 1995). SVR utilizes radial basis function kernels (Vert et al., 2004) and is calibrated for optimal cost and gamma hyperparameters, which govern training errors and degree of influence of a single training point. The SVR can be expressed as

$$\text{SVR}(x) = \sum_{i=1}^{N} \left(\alpha_i - \alpha_i^* \right) K\left(x_i, x \right) + b \,, \tag{1}$$

where N is the total number of support vectors, which corresponds to number of data points during training. α_i, α_i^* are Lagrangian multipliers, such that $\alpha_i \geq 0$ and $\alpha_i^* \leq 0$. K is the radial basis function kernel, such that

$$K\left(x_i, x_j \right) = \exp\left[-\frac{||x_i - x_j||^2}{2\sigma^2} \right] \,,$$

where $||x_i - x_j||$ is the Euclidian distance between feature vectors corresponding to the ith and jth input data points.

We trained the model using data from selected SNOTEL stations (described in Sect. 3.1) for 2017 and 2018. We fine-tuned the hyperparameters so that the model produces similar levels of accuracy when applied to observations from

the same stations for 2019 and 2020. The hyperparameter calibration process involved an exhaustive grid search technique, which systematically explored all possible combinations within predefined parameter ranges. Ultimately, we selected the hyperparameter configurations that resulted in the lowest root mean squared error between simulated and observed daily changes in SWE (dSWE) during both model training on observations from 2017 and 2018, and we tested the model on observations from 2019 and 2020.

2.3 Temperature threshold constraint and model wrapper function

Due to the instabilities of dSWE estimated by the SVR during rain–snow transition phases (described in Sect. 4.1), simulated dSWE at any day (t) values are constrained as follows:

$$\text{dSWE}_t = \begin{cases} \text{SVR}\left(x_t \right), & \text{if TAVG}_t \geq T_S \\ \text{PRCP}_t, & \text{if TAVG}_t < T_S \end{cases}, \tag{2}$$

where T_S is a 100 % rain–snow temperature threshold, with a default value of $-1\,°\text{C}$.

The dSWE estimates are then aggregated into daily SWE time series using the cumulative sum reset function as follows:

$$\text{SWE}_t = \begin{cases} 0, & \text{if } t = 0 \\ \max\left(\text{dSWE}_t + \text{SWE}_{t-1}, 0 \right), & \text{if } t > 0 \end{cases}. \tag{3}$$

3 Data

3.1 Data for training support vector regression

For training the SVR, we used the SNOTEL data listed in Table 2, the largest network of automated weather stations that collect data on snow water equivalent, precipitation, temperature, and other climatic variables. We used daily observations from 94 SNOTEL stations located in the contiguous United States for 2 hydrological years, 2017 and 2018. Figure 2 displays location of the selected stations, along with density distribution of their main geographical and topographical characteristics.

In the 1990s, the temperature observations from SNOTEL showed anomalous trends (Pepin et al., 2005), which were eventually attributed to a new temperature sensor (Oyler et al., 2015) installed with an incorrect equation algorithm. To correct for this bias, we applied a debiasing equation on SNOTEL temperature data, proposed by Brown et al. (2019), and using the metadata of affected stations (USDA, 2019).

SNOTEL precipitation gauges may also be susceptible to solid precipitation undercatch, especially when snowfall occurs in windy conditions (USDA, 2014). Scalzitti et al. (2016) provide a comprehensive review of the issues associated with precipitation undercatch, highlighting a reported undercatch ranging from 11 % for snowfall under
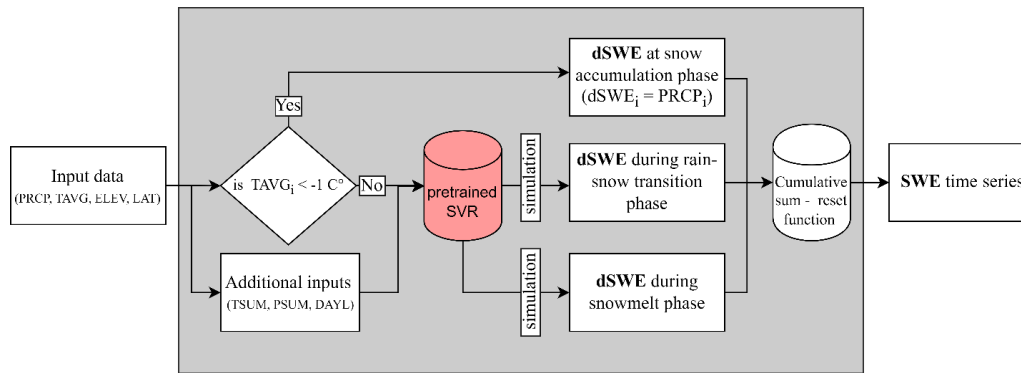
Figure 1. GEMS workflow. Model elements and abbreviations are described in the sub-sections that follow.

Table 1. Required forcing data for GEMS.

Input data	GEMS-4P	GEMS-5P	GEMS-6P	GEMS-7P
Precipitation (mm)	✓	✓	✓	✓
Mean daily temperature (°C)	✓	✓	✓	✓
Maximum daily temperature (°C)			✓	✓
Minimum daily temperature (°C)			✓	✓
Latitude (decimal degrees)	✓	✓	✓	✓
Elevation (m a.s.l.)	✓	✓	✓	✓
Heat–insolation index		✓		✓

$2 \, \mathrm{m \, s^{-1}}$ wind speed to more than 30 % during intense snowstorm events. To ensure data accuracy, we cleaned the training dataset by removing observations with inconsistencies between daily precipitation and snow mass accumulation. These inconsistencies refer to cases when the daily increase in SWE exceeded the reported daily precipitation.

The input data includes a heat–insolation index to account for the influence of topographic shading, which may result in a significant variability in the surface energy balance and therefore in snowmelt rate, particularly in complex terrain. We used the Continuous Heat–Insolation Load Index (CHILI), which approximates the effects of insolation and topographic shading on evapotranspiration and is determined by estimating insolation in the early afternoon at equinox Sun height (Theobald et al., 2015). The Google Earth Engine provides access to CHILI data on a global scale, with a horizontal resolution of 90 m. Since CHILI is a location-specific static characteristic, we also augmented the forcing data with day length, which is a time-varying variable estimated using latitude of a location and day of a year.

3.2 Data and procedure for evaluation of the model

The evaluation of the model performance followed a three-tiered structure.

First, we assessed the model performance using observations from SNOTEL stations that were not included in the training. The selection of stations for validation followed two main criteria. We excluded stations that exhibit precipitation undercatch, which we formulate as when SWE accumulated by March is greater than the accumulated precipitation during October to March. This approach enabled us to include more stations in the evaluation dataset, while excluding only those hydrological years that exhibited inconsistencies between these variables. We selected evaluation observations using this criterion without any specific threshold for the magnitude of inconsistencies, and we did not make corrections to the precipitation time series. Out of the filtered stations, we selected only stations that have complete daily observations for at least 5 water years, defined as October of the preceding year to September next year for any year from 2011 to 2022. The selection algorithm filtered 520 stations from a total of approximately 703 contiguous United States SNOTEL stations that had not been used for model training.

Second, we evaluated the model performance using snow and meteorological data from 10 reference stations, which were used in the Earth System Model–Snow Model Intercomparison Project (ESM–SnowMIP), hereinafter referred to as ESM–SnowMIP reference stations. Table 3 below provides descriptions of these sites.

Finally, we assessed the performance of the model using distributed large-scale climate data over the western Pamir in central Asia and central Andes regions with complex terrain (Fig. 3) by comparing observed and simulated snow cover. Both selected regions are characterized by semi-arid climate conditions in higher elevations and predominantly arid cli-
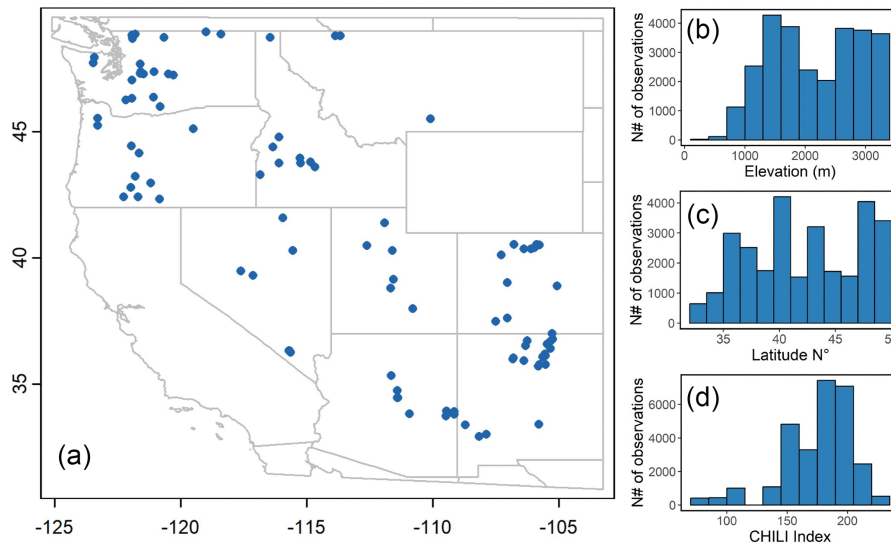
Figure 2. Location of SNOTEL stations used for training the SVR **(a)**, and their density distributions in terms of **(b)** elevation, **(c)** latitude, and **(d)** heat–insolation index.

Table 2. Climate and topographic data used to train the model.

Variable	Abbreviation	Source/reference
Daily change in snow water equivalent (mm)	dSWE	SNOTEL
Precipitation (mm)	PRCP	SNOTEL
Mean daily temperature (°C)	TAVG	SNOTEL
Maximum daily temperature (°C)	TMAX	SNOTEL
Minimum daily temperature (°C)	TMIN	SNOTEL
Rolling sum of temperature over preceding 3 d (°C)	TSUM	Calculated using TAVG
Cumulative sum of precipitation over preceding 3 d (mm)	PSUM	Calculated using PRCP
Day length (hours)	DAYL	Calculated as a function of latitude and day of a year (Forsythe et al., 1995)
Elevation (m a.s.l.)	ELEV	SNOTEL
Heat–insolation index	CHILI	Global Continuous Heat–Insolation Load Index (Theobald et al., 2015)

mate conditions in plains. We used temperature and precipitation data at 1 km resolution from CHELSA-W5E5 dataset (Karger et al., 2023) to force the model and compared the extent of SWE simulated during the two consecutive snow seasons between 2014 and 2016 with MODIS-derived snow cover retrievals using the cloud-gap-filled MOD10A1F product images (Riggs et al., 2019).

The evaluation metrics for single-point simulations across SNOTEL and ESM–SnowMIP reference sites consist of the Nash–Sutcliffe efficiency (NSE) coefficient (Nash and Sutcliffe, 1970), mean absolute percentage error in the peak SWE (maxSWE MAPE), bias of the simulated peak SWE

(maxSWE BIAS), and the difference in snow melt-out dates, as follows:

$$\text{NSE}\left(\text{SWE}, \widehat{\text{SWE}}\right) = 1 - \frac{\sum_{i=1}^{N(\text{days})}(\text{SWE}_i - \widehat{\text{SWE}}_i)^2}{\sum_{i=1}^{N(\text{days})}(\text{SWE}_i - \text{mean}(\text{SWE}_i))^2},$$

where SWE_i is the observed daily SWE. $\widehat{\text{SWE}}_i$ is the simulated daily SWE

$$\text{maxSWE MAPE}(y, \widehat{y}) = \frac{100\,\%}{N(\text{years})}\sum_{w=1}^{N(\text{years})}\frac{|y_w - \widehat{y}_w|}{y_w}$$

$$\text{maxSWE BIAS}(y, \widehat{y}) = \frac{100\,\%}{N(\text{years})}\sum_{w=1}^{N(\text{years})}\frac{y_w - \widehat{y}_w}{y_w},$$

Table 3. Geographic and climate characteristics of the ESM–SnowMIP reference stations.

Site name, country	Abbreviation	Latitude (° N)	Elevation (m a.s.l.)	Snow cover classification	Köppen climate classification
Col de Porte, France	CDP	45.3	1325	Alpine	Warm-summer humid continental climate
Old Aspen, Canada	OAS	53.63	600	Taiga	Warm-summer humid continental climate
Old Black Spruce, Canada	OBS	53.99	629	Taiga	Warm-summer humid continental climate
Old Jack Pine, Canada	OJP	53.92	579	Taiga	Warm-summer humid continental climate
Reynolds Mountain, USA	RME	43.19	2060	Alpine	Warm-summer humid continental climate
Sapporo, Japan	SAP	43.08	15	Maritime	Hot-summer continental climates
Senator Beck, USA	SNB	37.91	3714	Alpine	Polar and alpine (montane) climates
Swamp Angel, USA	SWA	37.91	3371	Alpine	Subarctic climate
Sodankylä, Finland	SOD	67.37	179	Taiga	Subarctic climate
Weissfluhjoch, Switzerland	WFJ	46.83	2536	Alpine	Polar and alpine (montane) climates

Source: Ménard et al. (2019).
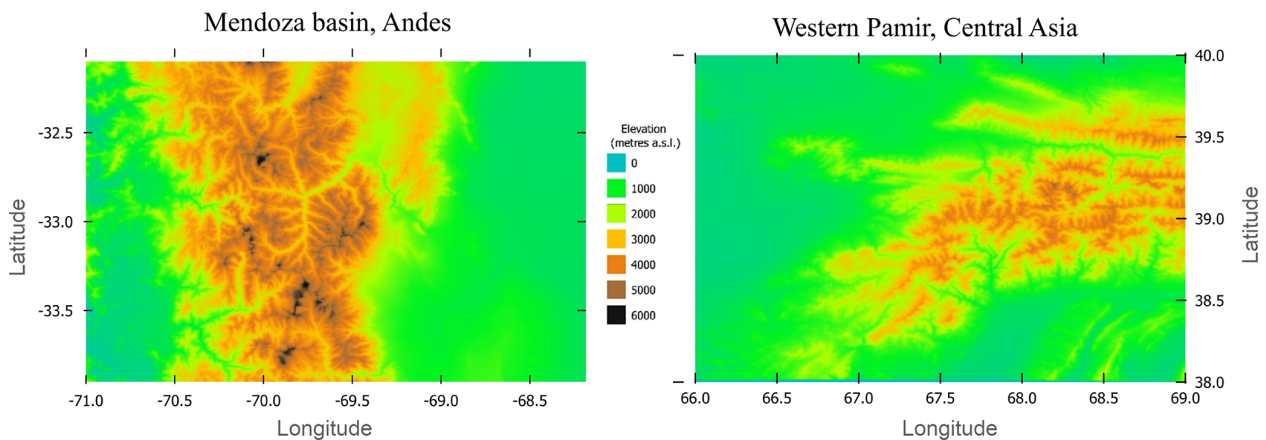
Figure 3. Selected regions for distributed snow modelling.

where y_w is the observed peak SWE in wth hydrological year. $\widehat{y}_w$ is the simulated peak SWE in wth hydrological year

$$\text{Snow melt-out date error} = \frac{1}{N(\text{years})} \sum_{w=1}^{N(\text{years})}$$

$$\text{mdate}_w - \widehat{\text{mdate}_w},$$

where mdate_w is the actual date of snow disappearance in wth hydrological year. $\widehat{\text{mdate}_w}$ is the date of the snow disappearance according to model simulations.

All simulations for the evaluation are implemented with the GEMS-7P version of the model that uses seven predictors (Table 1).

Section 4.7 compares the overall performance of the model's four different versions (GEMS-7P, GEMS-6P, GEMS-5P, and GEMS-4P).

4 Model evaluation

4.1 Observed and modelled daily changes in SWE across training and validation SNOTEL stations

Figure 4 compares observed and predicted dSWE values obtained by running the pretrained SVR using training, calibration, and validation datasets. The model yields plausible estimates of the dSWE, although the variance is greater at higher melt rates. There is a greater variance between simulated and observed values in the validation dataset, although it should be noted that it has a much larger number of observations compared to the training and calibration datasets (1.36 million, 28 600, and 32 600 observations, respectively), which results in more outliers. In each of the three instances, the slope of the linear regression between the observed and simulated values ranges between 1.03 to 0.99.

The validation dataset simulations exhibited a bigger proportion of outliers in the upper tile corresponding to snow accumulation phase (dSWE > 0). To determine the accuracy of the SVR's performance for this phase, we compared
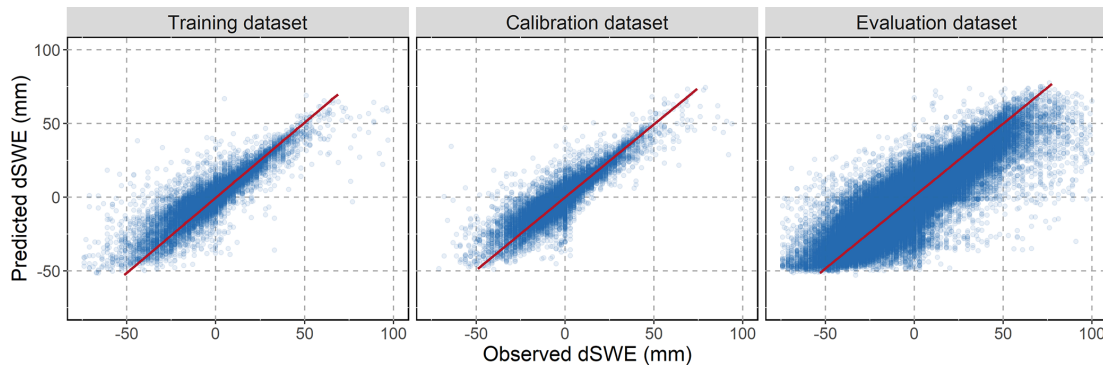
Figure 4. Predicted and observed dSWE values for training, calibration, and validation datasets. The red line represents the slope of the linear regression run on observed and predicted dSWE values.

model simulations using a sample of the validation dataset that includes observations with incremental changes in the SWE at the beginning of the snow season. Since the SNOTEL observations do not contain explicit information on the precipitation–snow transition, we decided to use a sample of the dataset to simulate the transition depending on climate inputs (temperature variables) and topographical characteristics (e.g. elevation). More specifically, we have filtered the SNOTEL observations that closely fall on the precipitation–snow transition phase by selecting observations that meet the following non-exhaustive main criteria: (1) observations for October or November when precipitation is non-zero; (2) average temperature (TAVG) is below 10 or above $-10\,°C$; and (3) accumulated SWE is below 20 mm. We then run the model using the obtained sample of observations and estimated solid fraction of precipitation simulated by the model, i.e. amount of dSWE estimated by the model with respect to precipitation amount.

Figure 5 depicts the rain-to-snow transition modelled using the metadata of the 520 validation SNOTEL stations. We conclude that average daily temperatures (TAVG) at which the model predicts precipitation to fall partially as snow may range from -5 to more than $5\,°C$ and have a relatively higher association with maximum temperature and elevation. The comparison also reveals that the simulations tend to underestimate snow accumulation, since in some cases the solid component of precipitation in simulations does not reach 100 %, even at temperatures below $-5\,°C$. In this regard, we have introduced a constraint (specified above in Sect. 3.4), which imposes that any daily precipitation after a certain temperature threshold (T_S) is considered to fall as 100 % snow. We set the default value of T_S as $-1\,°C$, which the simulations revealed to be the optimal common threshold, based on observations from the validation dataset.

Here it is important to note that the T_S constraint in the GEMS model differs from classical temperature-based partitioning methods, where the threshold defines precipitation in a binary way (either 100 % rainfall or 100 % snow). The model simulates snow–precipitation partitioning only until

the temperature drops below T_S, at which point any precipitation is regarded as 100 % snow. For example, when the average temperature (TAVG) is $0\,°C$, using the assimilated statistical relationships the model will likely simulate some portion of precipitation as snowfall. As illustrated in Fig. 5 at TAVG around of $0\,°C$, the model, on average, simulates around 75 % of precipitation as snowfall. Depending on other input variables, this ratio varied from approximately 25 % to as high as 95 %.

4.2 Model evaluation with independent SNOTEL stations

Figure 6 presents results of the model evaluation on multiannual data from the 520 independent SNOTEL stations with histograms and distribution maps of the four selected metrics. The model produces accurate simulations of SWE time series in most cases, with the median NSE for simulations across all the stations of 0.91, and for 84 % of the stations, the model achieved NSE of greater than or equal to 0.8. For 80 % of all stations, the maxSWE error (maxSWE MAPE) of the simulations is less than 20 %, with the median value for all stations being 14 %. The median error in the snow melt-out date was 4 d and did not exceed 10 d in 74 % of instances. We found no spatial associations for NSE values and maxSWE errors, while the bias for maxSWE and the snow melt-out date error tend to be larger in the western part of the study domain (in the vicinity of the Cascade Range, Oregon). Here the simulations overestimate maxSWE and the snow melt-out date by a larger margin. Another concentration of overestimation of simulated snow melt-out date occurs in stations located in the Sierra Nevada mountains. In contrast, the model systematically underestimates maxSWE in some stations in the northeastern part (Montana and Wyoming), where it consequently simulates earlier snow disappearance.

In addition to simulations generated with the default T_S value, we also examined the model's accuracy using T_S values calibrated to each SNOTEL station. We calibrated T_S for each of the stations with the objective of maximizing the
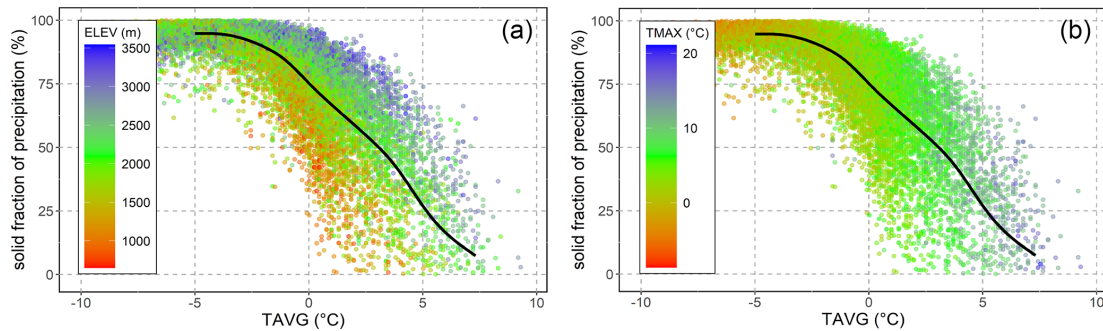
Figure 5. The rain–snow transition with respect to average temperature (TAVG) simulated by the pretrained SVR using metadata from the SNOTEL validation data. The two graphs illustrate the same simulations and highlight distributions of elevation **(a)** and maximum temperature **(b)**. The black line is the median of the resulting solid fraction of precipitation across the simulations.

Nash–Sutcliffe efficiency of the model's simulations with respect to observed SWE, and we bounded the range of calibrated T_S to -5 to $+5\,°C$. The results illustrated in Fig. 7 show that the station-adjusted modelling incrementally improves all evaluation metrics of the simulations result, though with a lesser impact on mean maxSWE error. Adjusted T_S values tend to be negative across the stations on mountain ranges, particularly across the Cascade Range and Sierra Nevada and Rocky mountains. A cluster of a few stations with positive T_S appear in the northeastern portion of the study region.

While the median of the adjusted T_S values for all stations agrees with its default threshold ($-1\,°C$), the density distribution also shows a high frequency of calibrated T_S resulting at the lowest bound of $-5\,°C$ (Fig. 7f). This suggests that, in cases where calibrated T_S values approach the lowest boundary, the model simulations might have been overcalibrated, resulting in error compensation. The overestimation of SWE at these locations can be attributed to several factors that the model does not account for, including effect of dense vegetation, wind-induced snow drift, sublimation, and rain-on-snow events which may be frequent phenomena in the mountain areas (Li et al., 2019; Boniface et al., 2015; Kirchner et al., 2014; Sexstone et al., 2018).

4.3   Model evaluation using ESM–SnowMIP reference station data

Table 4 presents obtained NSE, maxSWE MAP, and maxSWE bias values of the GEMS simulations using the ESM–SnowMIP reference stations, and Fig. 8 compares their observed and modelled SWE time series. The model performance at ESM–SnowMIP reference sites was robust for the majority of stations, with the T_S threshold set to $-1\,°C$ by default. In general, simulated SWE was more accurate for the stations located at higher elevations and characterized by higher snow accumulation rates (RME, CDP, WFJ, and SWA), except for SNB, which had the lowest NSE value (0.34) and the highest maxSWE error (17 %) among

all ESM–SnowMIP stations. The poor performance of the model for the SNB station is attributed to prevalence of wind-induced snow redistribution, which can reportedly reduce peak SWE on the site by up to 40 % (Landry et al., 2014). For the same reason, one of the largest SWE errors were recorded for the SNB site by the majority of models that participated in ESM–SnowMIP (Menard et al., 2021).

SWE simulations for SOD and SAP stations have NSE values of around 0.7 and maxSWE MAPE errors of 8 % and 18 %, respectively. It is important to note that in terms of latitude and thus the range of day lengths, the SOD station is situated much beyond the range of the data utilized to pretrain the GEMS model. In addition, since the global Continuous Heat–Insolation Load Index (CHILI) does not extend beyond the arctic circle. To estimate it for SOD, we used the nearest known value, assuming flat terrain, but acknowledge that our estimate may have some uncertainty. Regarding the SAP station, the performance of GEMS may be affected by the site's anomalous precipitation-phase partitioning, in which precipitation reportedly can fall as rain at low temperatures and as snow at temperatures over $5\,°C$ (Ménard et al., 2019).

The performance of the model exhibited notable disparities across three forested locations in Canada (OAS, OBS, and OJP). In comparison to other sites, the model's performance at these sites was relatively inferior, as indicated by NSE values ranging between 0.44 and 0.66 and maxSWE errors spanning from 15 % to 30 %. This observation suggests a diminished performance of the model in environments characterized by dense canopy interception.

For reference, Table 4 also provides the NSE of simulations produced by models that participated in ESM–SnowMIP. With the exception of the SNB site, ESM–SnowMIP simulations had lower NSE than those of GEMS simulations. However, a direct comparison between GEMS and ESM–SnowMIP simulations is not possible because evaluation data were not provided to the ESM–SnowMIP participants in advance, and rain–snow transitions were prescribed in the driving data (Ménard et al., 2019). ESM–
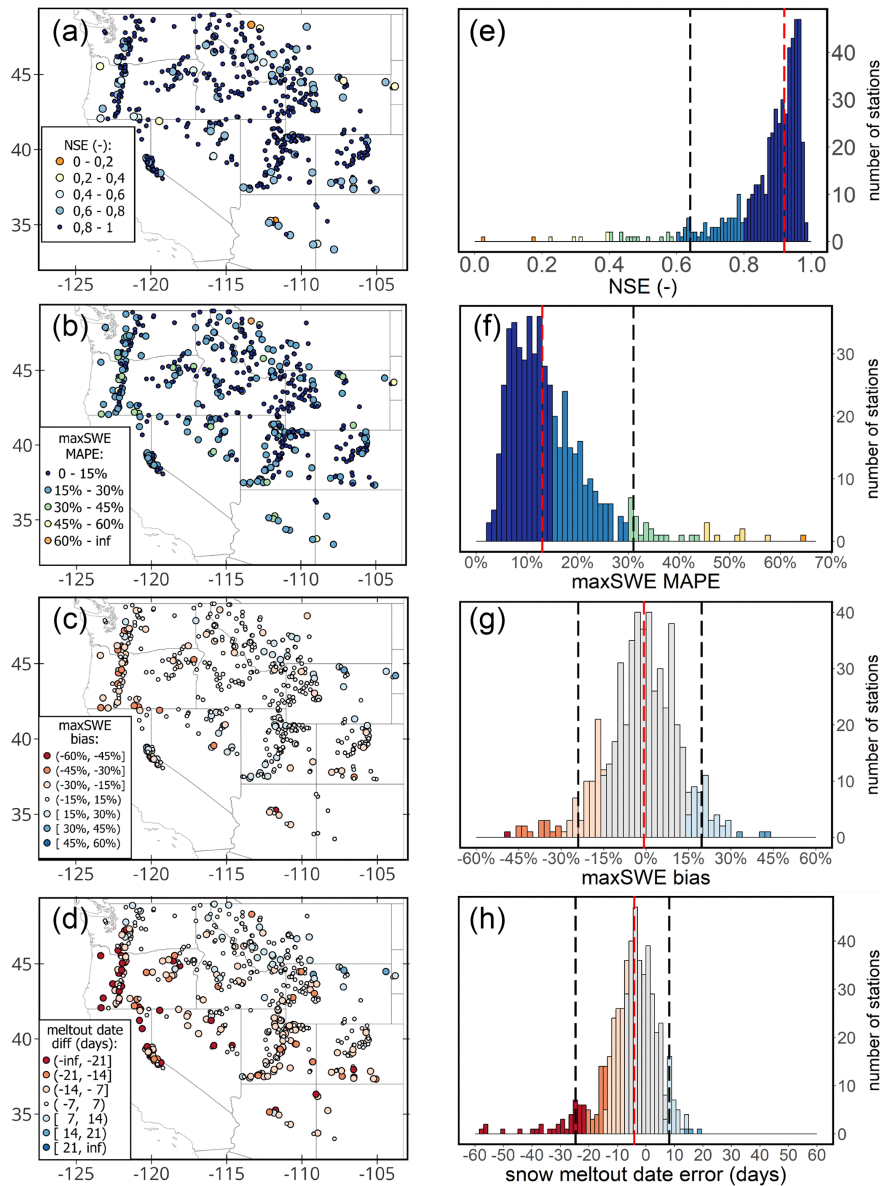
Figure 6. GEMS performance metrics for independent SNOTEL stations. Spatial distributions of the resultant **(a)** NSE, **(b)** maxSWE MAPE, **(c)** maxSWE bias, **(d)** snow melt-out date error, and corresponding histograms **(e–h)**. Vertical dashed red lines on the histograms denote the median across all stations; the vertical dashed black line correspond to the 5th percentile (and 95th percentile in the case of two-tailed distributions).

SnowMIP participants thus had no opportunity to enhance model performance by adjusting parameters.

4.4 Model evaluation for large-scale simulations

Figure 9 compares observed and simulated snow cover area for the selected western Pamir and Mendoza–Andes regions on a daily time step over two consecutive snow seasons. The primary objective of this analysis was to test and demonstrate the model's transferability to regions with complex terrain and without in situ SWE data. We assume that if the extent

of the simulated SWE aligns well with the remotely sensed snow cover, then the simulated SWE is likely to contain less uncertainty. This assumption is also based on the fact that remotely sensed snow cover is increasingly used for parameter calibration or uncertainty reduction in snow modules of hydrological models (e.g. Parajka and Blöschl, 2008; Gyawali and Bárdossy, 2022; Tong et al., 2022; Di Marco et al., 2021).

GEMS accurately reproduced seasonal cycles and interannual variations in the snow cover in the western Pamir and Mendoza–Andes region, which have distinctive seasonal patterns. The simulations capture short-term spikes in the
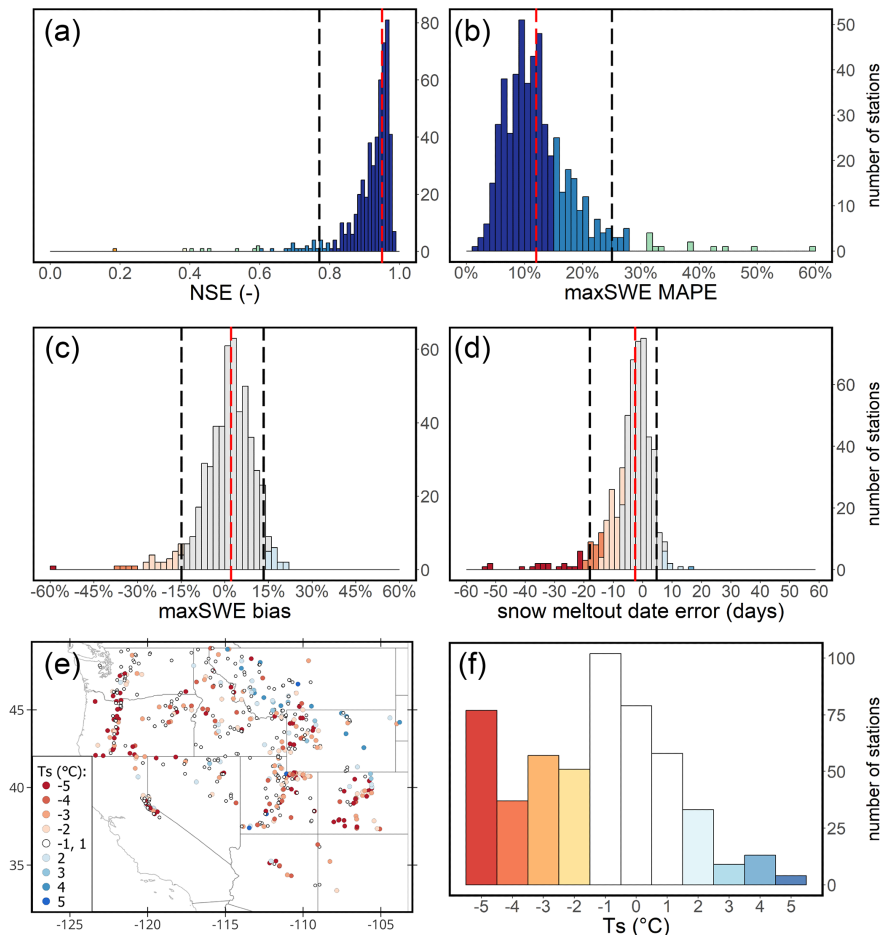
Figure 7. GEMS performance metrics for the independent SNOTEL stations with station-adjusted T_S threshold. **(a)** NSE, **(b)** maxSWE MAPE, **(c)** maxSWE bias, and **(d)** snow melt-out date error. The bottom map **(e)** and histogram **(f)** show the density and spatial distribution of the adjusted T_S values.

Table 4. GEMS performance metrics for the ESM–SnowMIP reference stations.

Station	GEMS model			ESM–SnowMIP models
	NSE	maxSWE MAPE (%)	maxSWE BIAS (%)	max NSE
CDP	0.84	14	0	0.6
OAS	0.6	15	−13	0.24
OBS	0.44	29	−29	0.18
OJP	0.66	27	−30	0.41
RME	0.8	13	−13	0.72
SAP	0.72	17	3	0.47
SNB	0.34	17	−13	0.46
SOD	0.68	8	6	0.68
SWA	0.85	15	14	0.6
WFJ	0.85	14	4	0.64
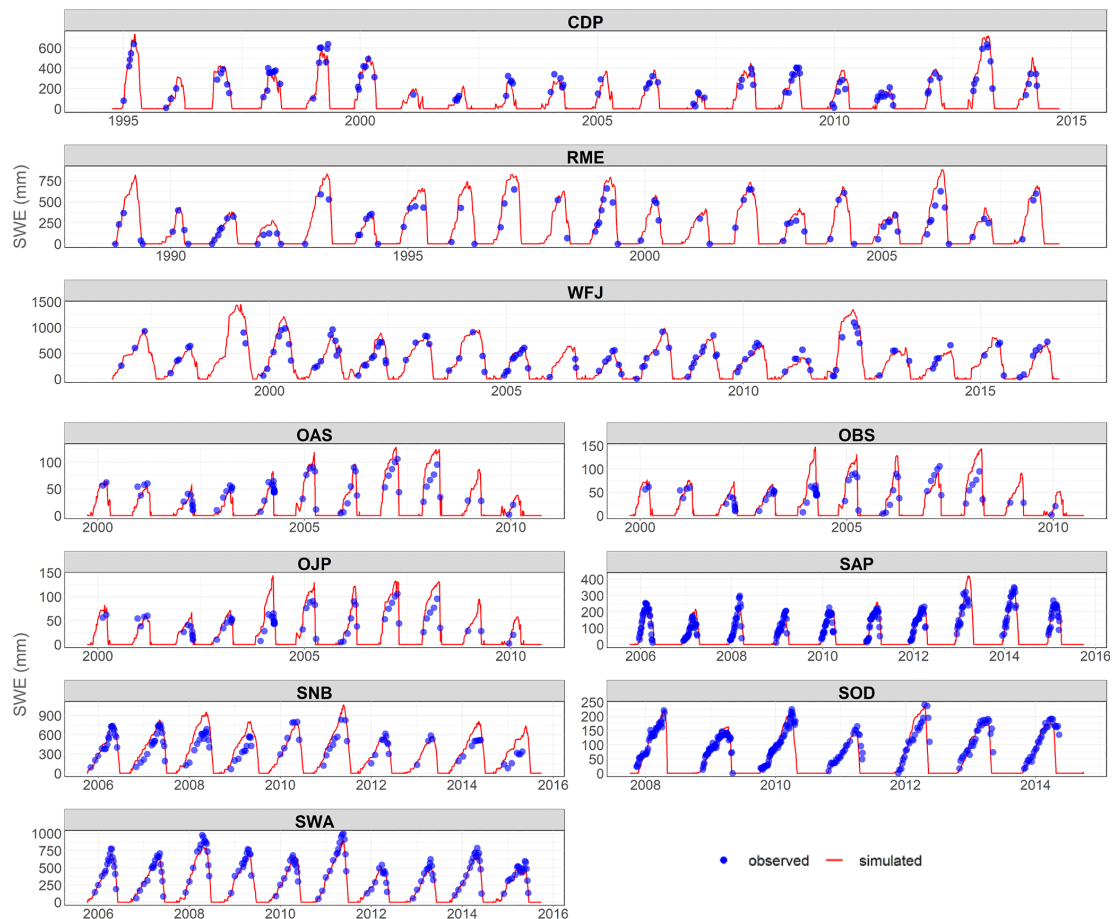
Figure 8. Observed and modelled SWE at the ESM–SnowMIP reference stations (with the default T_S threshold).

snow cover extent in the middle of the snow seasons over the Pamir. Overall pixel-wise accuracy of snow/no-snow detection for both regions was 92 %, while the class-balanced accuracy, which takes into account the balance of class distribution (Branco et al., 2016), was 87 % on average.

All validation sites used previously are in the Northern Hemisphere because we were unable to locate representative station-based snow and climate forcing data for model evaluation in the Southern Hemisphere. The evaluation of the model in the Mendoza–Andes region implies that the model may have comparable performance for locations in the Southern Hemisphere.

4.5 Relative importance of climate and topographic variables

We conducted a permutation-based feature importance analysis to determine how individual input variables affect dSWE simulation. The method randomly shuffles input data and compares the model's baseline performance on the original dataset to performance after permuting a feature's values (Fisher et al., 2019; Greenwell et al., 2018). We applied the permutation-based feature importance analysis on the entire

training dataset of the independent SNOTEL stations, as well as its subsamples representing snow accumulation or melt phases. Figure 10 illustrates the obtained variable importance scores.

The results unequivocally identified precipitation and average temperature followed by day length as the most significant variables, but they also demonstrate that their importance varies considerably depending on the phase considered. For snow accumulation, precipitation is by far the most obvious and significant variable, followed by a wide margin by maximum temperature. In contrast, the model relies heavily on average temperature and day length to predict snowmelt, followed by precipitation and other remaining variables, again by a wide margin. At first glance, the results suggest that topographic variables are among the least influential, but it should be noted that their significance is assessed in relation to other variables, some of which, such as precipitation and temperature, are more fundamental for accurate snowpack estimation (Günther et al., 2019). Furthermore, climate predictors can be highly variable, whereas topographic features are constant per each location, which predetermines insufficient variability in these predictors in the
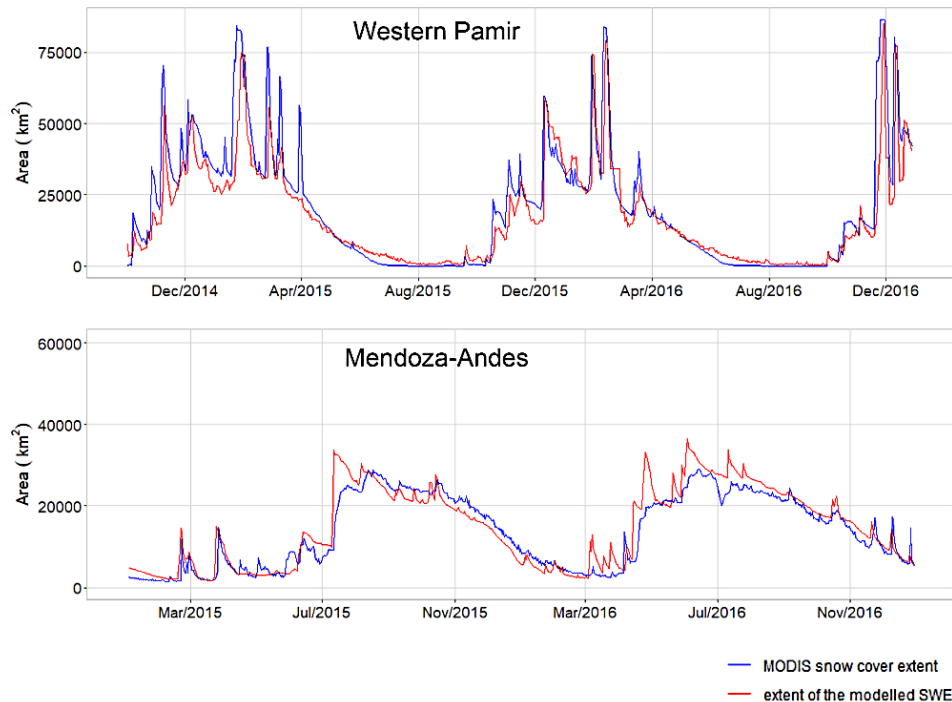
Figure 9. Observed and simulated snow cover area for western Pamir and Mendoza–Andes region.

dataset and thus contributes to a wider gap in their relative importance in comparison with climate variables.

4.6 Climatic and topographic attributes of locations where the model exhibited lower accuracy

In order to evaluate model uncertainty, we filtered the SNO-TEL stations into two groups based on their NSE values, namely one group from the first quartile and another group from the fourth quartile of NSE values across all validation SNOTEL stations. We then calculated probability distribution densities for several climatic and topographic characteristics (presented in Fig. 11) for each group to compare how stations with relatively poorer model performance differ from those with good model performance.

Accordingly, there is a higher likelihood that a station where the GEMS shows relatively inferior performance typically yields lower seasonal snowpack and has higher average seasonal temperatures. In addition, stations with poor model performance tend to have higher diurnal fluctuations during the snow season. We have detected minor differences between two groups of stations in terms of average elevation or distribution of heat–insolation indices. Despite not using station latitude in the model as a direct input (it is required to estimate day length for the location), the comparison suggests that there was a slightly higher proportion of poorly performing stations at lower latitudes.

These distinguishing characteristics of poorly performing stations in some instances are not mutually exclusive. For ex-

ample, locations with higher seasonal temperatures usually tend to have lower seasonal SWE peaks under identical conditions. Similarly, lower latitudes in the western USA have generally greater diurnal air temperature variations. We hypothesize that the performance of the model under such climatic conditions could be enhanced by incorporating more respective observations into the training dataset, which apparently included fewer SNOTEL stations from the southern part of the training domain (see Fig. 2c).

4.7 Performance of GEMS model under different input requirements

To evaluate how the model performance depends on a number and type of input data (see Table 1), we compared simulations of the three versions of GEMS using the SNOTEL validation dataset. Overall, the incorporation of diurnal temperature range and heat–insolation index enhances simulation accuracy as measured by a smaller interquartile range of NSE and maxSWE error (Fig. 12). Compared to utilizing only the maximum and minimum temperatures, the heat–insolation index is a predictor that appears to modestly improve model accuracy. This improvement is evident because compared to GEMS-6P, GEMS-5P exhibits somewhat better performance across the four metrics used.

Besides, GEMS-7P and GEMS-5P have a tighter range between the minimum and maximum NSE and maxSWE error. However, there is no discernible difference in the snow melt-out date and maximum SWE bias across the three model
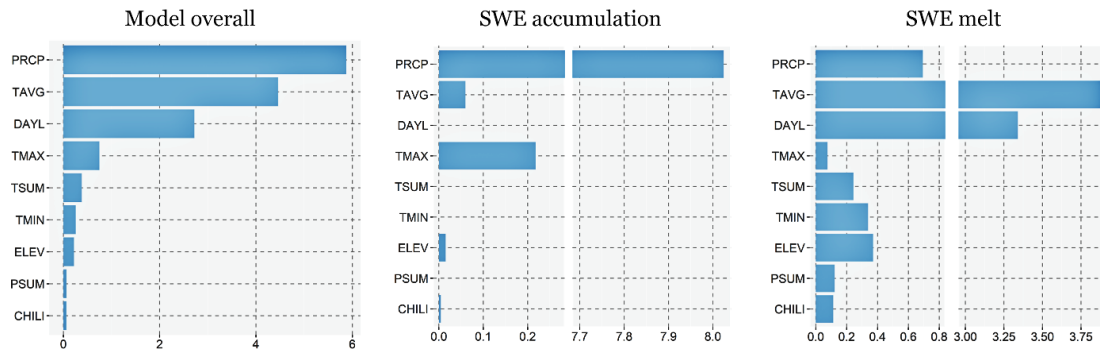
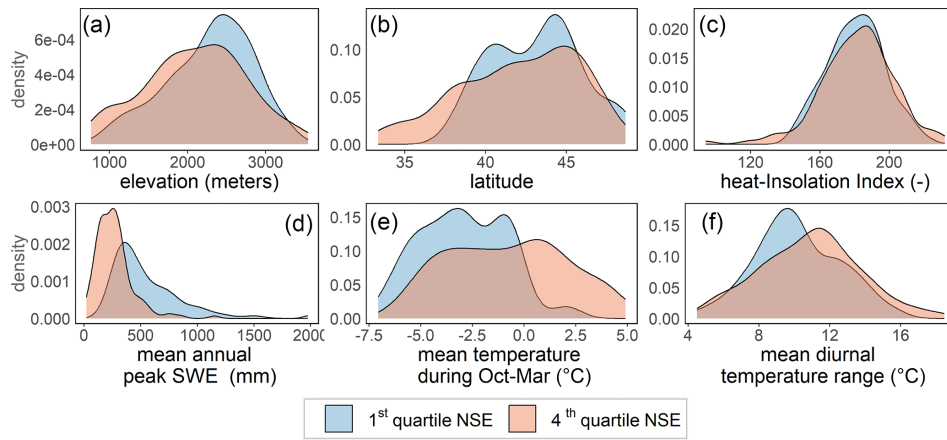**Figure 10.** Relative importance of model inputs during SWE accumulation and melt phases.

Figure 11. Probability density distributions of topographic and climatic characteristics of the SNOTEL stations, where the model shows higher and lower performance in terms of NSE.

versions. Although GEMS-4P has a slightly lower NSE and maxSWE error accuracy, its overall performance is still robust, and it has the benefit of requiring fewer inputs (only precipitation, average temperature, elevation, and latitude).

Running any of the three versions of the model on a desktop computer using a single CPU core (Intel i7) was shorter than 6 s for 20-year-long Weissfluhjoch station data, which approximates to 0.3 s per site year. An ongoing experiment (not shown here) suggests that the computation time can be reduced by about 30 % through improved sampling of the training data used to develop the model, a modification that will be implemented in the updated version of GEMS.

5   Model limitations

Instances of less consistent simulations generated by the model can arise from various sources of uncertainty, including internal uncertainty within the model, as well as uncertainty in input data and unaccounted external factors.

One of the major limitations of the model is that it does not account for vegetation, which is known to have a complex and divergent effect on snow accumulation and melt under different climate conditions (Dickerson-Lange et al., 2021; Sun et al., 2022). Because most SNOTEL stations are situated in forest clearings or open bushes, we initially assumed the training sample locations to be free of canopy obstruction. Using Google Earth, a visual check of the stations used in both the training and validation samples reveals, however, that some sites can be intercepted by the tree canopies in their surroundings. In addition, we have detected the shadowing of some snow pillows by the dense forests that surround them. Both phenomena are possible sources of model uncertainty, as also evidenced from relatively lower performance of the model for three forested ESM–SnowMIP sites in Canada (OAS, OBS, and OJP), and future model development should try to incorporate vegetation effects.

Based on a comparison of high-performing and low-performing site simulations, the model may be less accurate at simulating shallow snow in warm sites at lower elevations. When these factors combine with large diurnal temperature fluctuations, model simulations may even become more distorted. These issues could be resolved with a more sophisticated sampling strategy and by incorporating additional observations into the training of the model. It remains unclear, however, whether an improved sampling strategy could also
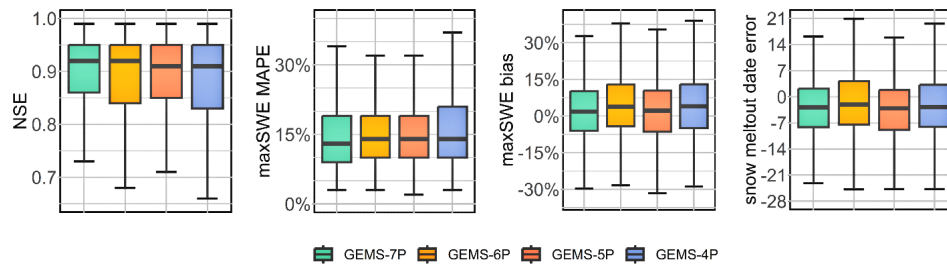
Figure 12. Comparison of performance across three GEMS models. The minimum and maximum limits of the box plots correspond to first $Q - 1.5 \cdot$ IQR (interquartile range) and third $Q + 1.5 \cdot$ IQR, respectively.

better approximate rain-on-snow effects, as these are driven by dynamic processes of energy exchanges across snow layers that the model does not capture for.

The model's parsimonious design, which relies only on precipitation and temperature variables as climate inputs, also precludes the incorporation of wind- or gravity-induced snow redistribution, which may compromise the accuracy of single-point simulations for wind-exposed sites.

When temperature is below the $-1\,°C$ T_{S} threshold and precipitation is $0\,mm$, GEMS will automatically estimate daily change in SWE as $0\,mm$. The model thus fails to account for snow sublimation, which can occur even when temperatures are below freezing. This differs from snow models based on energy balance, which can estimate snow sublimation. Furthermore, the evaluation on the SNOTEL dataset suggests that significant adjustments of the T_{S} threshold imposes a risk of error compensation due to overcalibration. Therefore, we recommend adhering to the default value of T_{S} $(-1\,°C)$, unless local precipitation–snow partitioning patterns are well understood.

As discussed in Sect. 4.6 and also evidenced from the evaluation on ESM–SnowMIP sites, the model demonstrates relatively better performance in mountainous areas compared to lower elevations. However, the training dataset used to elaborate the model may be less representative of locations with very low CHILI indices (Fig. 2d). Low CHILI indices often correspond to sites significantly shadowed by terrain or situated at higher latitudes or both. This discrepancy may be an additional source of model uncertainty.

6   Summary and conclusions

We present a computationally efficient model that emulates snow mass accumulation and melting, using only a few climate and topographic inputs. The absence of the explicit need for calibration is the most distinctive aspect of the GEMS model, with a $100\,\%$ rain–snow transition temperature threshold (T_{S}) being the only parameter that can be modified; though, in most validation cases, robust simulations were obtained just using the default T_{S} value. Despite its parsimony and no extensive calibration options, the model

achieves robust transferability across a variety of climate and geographic conditions.

The main motivation behind the development of GEMS was to balance the trade-off between complexity, data requirement, and transferability, which can be helpful for operational monitoring and hydrological modelling in data-scarce domains. The emulator was developed by training a machine learning model on daily changes in snow water equivalent as a response to daily climate inputs and diverse topographic features. Despite the dynamic nature of snow processes, our simplified, static approach effectively captured the impact of precipitation, temperature, and topography on snowmelt, as indicated by the validation results. This corroborates the conclusion of several intercomparison studies that model complexity is not necessarily a predeterminant of its performance (Essery et al., 2013; Magnusson et al., 2015; Menard et al., 2021).

The model evaluation suggests that GEMS achieves comparable performance to physical snow models, as evidenced by comparing with simulations from ESM–SnowMIP. A more appropriate comparison might necessitate the adjustment of physical model parameters, which was not investigated in ESM–SnowMIP. Nevertheless, the evaluation outcomes allow us to conclude that, at the very least, GEMS with its default T_{S} parameter exhibits superior spatial transferability compared to physical models with unadjusted parameters.

In addition to avoiding computationally demanding calibration, GEMS may also help to address the equifinality of model parameters that is pertinent to hydrological and snow modelling. The challenge of equifinality is particularly pronounced in hydrological modelling, where even relatively simple snow models require calibration of at least two parameter, namely the precipitation–snow threshold and the degree day melt factor. Considering that there are many other parameters for the remaining components of a hydrological model, it is easy to end up with multiple combinations of optimal parameters. In contrast, GEMS shows a generally plausible performance in diverse climatic and topographic conditions using the default value of T_{S}.

One difference between GEMS and physics-based models lies in the number of outputs they generate. While GEMS is

specifically designed to simulate only SWE, comprehensive physics-based snow models produce a broader spectrum of outputs that provide valuable insights into other snow properties. We assume that machine learning could become helpful in modelling some of these snow properties. For example, previous studies have shown how simple empirical models can effectively derive snow depth from SWE measurements, and vice versa (Aschauer et al., 2023; Hill et al., 2019). We assume that a similar approach to GEMS could be scalable for estimating snow depth by incorporating additional variables, such as snow age.

Machine learning is gaining importance in snow modelling, with existing applications predominantly focusing on snowpack interpolation or the detection of its instantaneous state through the assimilation of ground truth and active satellite radar data. GEMS provides a modelling framework similar to traditional snow modelling approaches by simulating snowpack in a temporally progressive manner and leveraging climate and topographic inputs commonly used in snow models. Moreover, the revealed variable importance aligns with the general physics governing how climate variables affect snowpack accumulation and melt. Some recent studies employing machine learning methods (Vafakhah et al., 2022; Duan et al., 2023) also simulate snowpack in a temporal manner and demonstrate robust performance, though spatial extrapolation limits of those algorithms remain unclear. Another recent study (Wang et al., 2022) presents promising results for a deep-learning-based approach, showcasing its superior spatial transferability compared to enhanced temperature index model across the United States. Nevertheless, the applicability of these models beyond their targeted regions may be questionable, due to dependance on climate inputs or locally specific data that may not be available elsewhere. From these perspectives, GEMS offers a higher degree of parsimony in terms of required input variables and, more importantly, a proven ability to generalize outside of the training domain.

We have tested several other data-driven techniques for the model development, including multivariate linear regression, Gaussian process, random forests, and gradient boosting machines (not shown here). When evaluating on the training dataset, the performance of most models was either lower than or equivalent to SVR; however, even in the latter case, their accuracy on the evaluation dataset was worse. Experiments in other fields indicate that SVR has relatively better extrapolation potential on unseen data (Horn and Schulz, 2011; Kim and Kim, 2019), which may explain why it outperformed other algorithms. We have not examined neural network algorithms, since they require more computer resources during training, and evidence suggests that they tend to underperform relative to other machine learning (ML) techniques when applied to tabular data (Borisov et al., 2022; Shwartz-Ziv and Armon, 2022). To make definitive judgements with regard to the performances of different machine learning algorithms, however, would require a more exten-

sive intercomparison experiment which is outside the scope of this paper.

Future development of GEMS may aim at addressing vegetation effects and improving model performance for shallow snowpack in warm sites. Including sublimation and rain-on-snow effects may be possible but may inevitably lead to increased complexity of the model. Another promising aspect of model improvement involves further reduction in the computational costs. At least to some extent, these improvements may be achieved through a more careful selection and sampling of the training dataset used to develop the model. In addition to these imperatives, further work may also concentrate on extending a similar framework for modelling other snow properties, such as snow depth and albedo.

Author contributions. AU and DM designed the study. AU performed computations. RE provided feedback on the model evaluation. All authors contributed to the writing and review of the paper. DM supervised the project.

Disclaimer. Publisher's note: Copernicus Publications remains neutral with regard to jurisdictional claims made in the text, published maps, institutional affiliations, or any other geographical representation in this paper. While Copernicus Publications makes every effort to include appropriate place names, the final responsibility lies with the authors.

2020), vip (Greenwell and Boehmke, 2020), and dplyr (Wickham et al., 2023).

References

Armstrong, R. L., Rittger, K., Brodzik, M. J., Racoviteanu, A., Barrett, A. P., Khalsa, S.-J. S., Raup, B., Hill, A. F., Khan, A. L., Wilson, A. M., Kayastha, R. B., Fetterer, F., and Armstrong, B.: Runoff from glacier ice and seasonal snow in High Asia: separating melt water sources in river flow, Reg. Environ. Change, 19, 1249–1261, https://doi.org/10.1007/s10113-018-1429-0, 2019.

Aschauer, J., Michel, A., Jonas, T., and Marty, C.: An empirical model to calculate snow depth from daily snow water equivalent: SWE2HS 1.0, Geosci. Model Dev., 16, 4063–4081, https://doi.org/10.5194/gmd-16-4063-2023, 2023.

Awad, M. and Khanna, R.: Support Vector Regression, in: Efficient Learning Machines, Apress, Berkeley, CA, 67–80, https://doi.org/10.1007/978-1-4302-5990-9_4, 2015.

Barnett, T. P., Adam, J. C., and Lettenmaier, D. P.: Potential impacts of a warming climate on water availability in snow-dominated regions, Nature, 438, 303–309, https://doi.org/10.1038/nature04141, 2005.

Bavera, D., Bavay, M., Jonas, T., Lehning, M., and De Michele, C.: A comparison between two statistical and a physically-based model in snow water equivalent mapping, Adv. Water Resour., 63, 167–178, https://doi.org/10.1016/j.advwatres.2013.11.011, 2014.

Beniston, M.: Extreme climatic events and their impacts: Examples from the swiss alps, in: Climate Extremes and Society, edited by: Diaz, H. and Park, G., Cambridge University Press, Cambridge, England, 147–164, https://doi.org/10.1017/CBO9780511535840.010, 2008.

Beven, K.: Prophecy, reality and uncertainty in distributed hydrological modelling, Adv. Water Resour., 16, 41–51, https://doi.org/10.1016/0309-1708(93)90028-E, 1993.

Beven, K.: A manifesto for the equifinality thesis, J. Hydrol., 320, 18–36, https://doi.org/10.1016/j.jhydrol.2005.07.007, 2006.

Boniface, K., Braun, J. J., McCreight, J. L., and Nievinski, F. G.: Comparison of Snow Data Assimilation System with GPS reflectometry snow depth in the Western United States, Hydrol. Process., 29, 2425–2437, https://doi.org/10.1002/hyp.10346, 2015.

Borisov, V., Leemann, T., Seßler, K., Haug, J., Pawelczyk, M., and Kasneci, G.: Deep Neural Networks and Tabu-

lar Data: A Survey, IEEE T. Neur. Net. Learn., 1–21, https://doi.org/10.1109/TNNLS.2022.3229161, 2022.

Branco, P., Torgo, L., and Ribeiro, R. P.: A Survey of Predictive Modeling on Imbalanced Domains, ACM Comput. Surv., 49, 31, https://doi.org/10.1145/2907070, 2016.

Brown, C. R., Domonkos, B., Brosten, T., DeMarco, T., and Rebentisch, A.: Transformation of the SNOTEL Temperature Record – Methodology and Implications, 87th Annual Western Snow Conference, https://www.nrcs.usda.gov/sites/default/files/2023-04/TransformationofSNOTELTemperature-MethodologyandImplications.pdf (last access: 31 January 2024), 2019.

Broxton, P. D., van Leeuwen, W. J. D., and Biederman, J. A.: Improving Snow Water Equivalent Maps With Machine Learning of Snow Survey and Lidar Measurements, Water Resour. Res., 55, 3739–3757, https://doi.org/10.1029/2018WR024146, 2019.

Carletti, F., Michel, A., Casale, F., Burri, A., Bocchiola, D., Bavay, M., and Lehning, M.: A comparison of hydrological models with different level of complexity in Alpine regions in the context of climate change, Hydrol. Earth Syst. Sci., 26, 3447–3475, https://doi.org/10.5194/hess-26-3447-2022, 2022.

Chase, R. J., Harrison, D. R., Burke, A., Lackmann, G. M., and McGovern, A.: A Machine Learning Tutorial for Operational Meteorology. Part I: Traditional Machine Learning, Weather Forecast., 37, 1509–1529, https://doi.org/10.1175/WAF-D-22-0070.1, 2022.

Daudt, R. C., Wulf, H., Hafner, E. D., Bühler, Y., Schindler, K., and Wegner, J. D.: Snow depth estimation at country-scale with high spatial and temporal resolution, ISPRS J. Photogramm., 197, 105–121, https://doi.org/10.1016/j.isprsjprs.2023.01.017, 2023.

Dickerson-Lange, S. E., Vano, J. A., Gersonde, R., and Lundquist, J. D.: Ranking Forest Effects on Snow Storage: A Decision Tool for Forest Management, Water Resour. Res., 57, e2020WR027926, https://doi.org/10.1029/2020WR027926, 2021.

Di Marco, N., Avesani, D., Righetti, M., Zaramella, M., Majone, B., and Borga, M.: Reducing hydrological modelling uncertainty by using MODIS snow cover data and a topography-based distribution function snowmelt model, J. Hydrol., 599, 126020, https://doi.org/10.1016/j.jhydrol.2021.126020, 2021.

Duan, S., Ullrich, P., Risser, M., and Rhoades, A.: Using Temporal Deep Learning Models to Estimate Daily Snow Water Equivalent over the Rocky Mountains, ESS Open Archive [preprint], https://doi.org/10.1002/essoar.10511321.2, 2023.

Essery, R.: Understanding and getting started with physically based snowmelt models, https://iahs.info/uploads/Commissions/ICSIH/ICSIHUnderstandingphysicallybasedsnowmeltmodels.pdf (last access: 29 January 2024), 2019.

Essery, R., Morin, S., Lejeune, Y., and B Ménard, C.: A comparison of 1701 snow models using observations from an alpine site, Adv. Water Resour., 55, 131–148, https://doi.org/10.1016/j.advwatres.2012.07.013, 2013.

Fisher, A., Rudin, C., and Dominici, F.: All Models are Wrong, but Many are Useful: Learning a Variable's Importance by Studying an Entire Class of Prediction Models Simultaneously, J. Mach. Learn. Res., 20, 1–81, 2019.

Forsythe, W. C., Rykiel, E. J., Stahl, R. S., Wu, H., and Schoolfield, R. M.: A model comparison for daylength as a function of latitude and day of year, Ecol. Model., 80, 87–95, https://doi.org/10.1016/0304-3800(94)00034-F, 1995.

Greenwell, B. M. and Boehmke, B. C.: Variable Importance Plots - An Introduction to the vip Package, R J., 12, 343, https://doi.org/10.32614/RJ-2020-013, 2020.

Greenwell, B. M., Boehmke, B. C., and McCarthy, A. J.: A Simple and Effective Model-Based Variable Importance Measure, arXiv preprint arXiv:1805.04755, 1–27, 2018

Günther, D., Marke, T., Essery, R., and Strasser, U.: Uncertainties in Snowpack Simulations – Assessing the Impact of Model Structure, Parameter Choice, and Forcing Data Error on Point-Scale Energy Balance Snow Model Performance, Water Resour. Res., 55, 2779–2800, https://doi.org/10.1029/2018WR023403, 2019.

Günther, D., Hanzer, F., Warscher, M., Essery, R., and Strasser, U.: Including Parameter Uncertainty in an Intercomparison of Physically-Based Snow Models, Front. Earth Sci., 8, https://doi.org/10.3389/feart.2020.542599, 2020.

Gyawali, D. R. and Bárdossy, A.: Development and parameter estimation of snowmelt models using spatial snow-cover observations from MODIS, Hydrol. Earth Syst. Sci., 26, 3055–3077, https://doi.org/10.5194/hess-26-3055-2022, 2022.

Hernanz, A., García-Valero, J. A., Domínguez, M., and Rodríguez-Camino, E.: A critical view on the suitability of machine learning techniques to downscale climate change projections: Illustration for temperature with a toy experiment, Atmos. Sci. Lett., 23, e1087, https://doi.org/10.1002/asl.1087, 2022.

Hijmans, R. J.: terra: Spatial Data Analysis, https://cran.r-project.org/package=terra (last access: 29 January 2024), 2023.

Hill, D. F., Burakowski, E. A., Crumley, R. L., Keon, J., Hu, J. M., Arendt, A. A., Wikstrom Jones, K., and Wolken, G. J.: Converting snow depth to snow water equivalent using climatological variables, The Cryosphere, 13, 1767–1784, https://doi.org/10.5194/tc-13-1767-2019, 2019.

Hock, R.: Temperature index melt modelling in mountain areas, J. Hydrol., 282, 104–115, https://doi.org/10.1016/S0022-1694(03)00257-9, 2003.

Horn, J. E. and Schulz, K.: Spatial extrapolation of light use efficiency model parameters to predict gross primary production, J. Adv. Model. Earth Sy., 3, https://doi.org/10.1029/2011MS000070, 2011.

Immerzeel, W. W., Lutz, A. F., Andrade, M., Bahl, A., Biemans, H., Bolch, T., Hyde, S., Brumby, S., Davies, B. J., Elmore, A. C., Emmer, A., Feng, M., Fernández, A., Haritashya, U., Kargel, J. S., Koppes, M., Kraaijenbrink, P. D. A., Kulkarni, A. V., Mayewski, P. A., Nepal, S., Pacheco, P., Painter, T. H., Pellicciotti, F., Rajaram, H., Rupper, S., Sinisalo, A., Shrestha, A. B., Viviroli, D., Wada, Y., Xiao, C., Yao, T., and Baillie, J. E. M.: Importance and vulnerability of the world's water towers, Nature, 577, 364–369, https://doi.org/10.1038/s41586-019-1822-y, 2020.

Karger, D. N., Lange, S., Hari, C., Reyer, C. P. O., and Zimmermann, N. E.: CHELSA-W5E5 v1.0: W5E5 v1.0 downscaled with CHELSA v2.0, ISIMIP Repository [data set], https://doi.org/10.48364/ISIMIP.836809.3, 2022.

Karger, D. N., Lange, S., Hari, C., Reyer, C. P. O., Conrad, O., Zimmermann, N. E., and Frieler, K.: CHELSA-W5E5: daily 1 km meteorological forcing data for climate impact studies, Earth Syst. Sci. Data, 15, 2445–2464, https://doi.org/10.5194/essd-15-2445-2023, 2023.

Kim, M. and Kim, J.: Extending the coverage area of regional ionosphere maps using a support vector machine algorithm, Ann. Geophys., 37, 77–87, https://doi.org/10.5194/angeo-37-77-2019, 2019.

King, F., Erler, A. R., Frey, S. K., and Fletcher, C. G.: Application of machine learning techniques for regional bias correction of snow water equivalent estimates in Ontario, Canada, Hydrol. Earth Syst. Sci., 24, 4887–4902, https://doi.org/10.5194/hess-24-4887-2020, 2020.

Kirchner, P. B., Bales, R. C., Molotch, N. P., Flanagan, J., and Guo, Q.: LiDAR measurement of seasonal snow accumulation along an elevation gradient in the southern Sierra Nevada, California, Hydrol. Earth Syst. Sci., 18, 4261–4275, https://doi.org/10.5194/hess-18-4261-2014, 2014.

Kraaijenbrink, P. D. A., Stigter, E. E., Yao, T., and Immerzeel, W. W.: Climate change decisive for Asia's snow meltwater supply, Nat. Clim. Change, 11, 591–597, https://doi.org/10.1038/s41558-021-01074-x, 2021.

Kumar, M., Marks, D., Dozier, J., Reba, M., and Winstral, A.: Evaluation of distributed hydrologic impacts of temperature-index and energy-based snow models, Adv. Water Resour., 56, 77–89, https://doi.org/10.1016/j.advwatres.2013.03.006, 2013.

Landry, C. C., Buck, K. A., Raleigh, M. S., and Clark, M. P.: Mountain system monitoring at Senator Beck Basin, San Juan Mountains, Colorado: A new integrative data source to develop and evaluate models of snow and hydrologic processes, Water Resour. Res., 50, 1773–1788, https://doi.org/10.1002/2013WR013711, 2014.

Li, D., Lettenmaier, D. P., Margulis, S. A., and Andreadis, K.: The Role of Rain-on-Snow in Flooding Over the Conterminous United States, Water Resour. Res., 55, 8492–8513, https://doi.org/10.1029/2019WR024950, 2019.

Link, T., Jonas, T., Mcphee, J., Skiles, M., and Marks, D.: Understanding strengths and limitations of temperature-index snowmelt models, https://iahs.info/uploads/Commissions/ICSIH/ICSIHsnowmodelingarticleFINAL.pdf (last access: 31 January 2024), 2019.

Magnusson, J., Farinotti, D., Jonas, T., and Bavay, M.: Quantitative evaluation of different hydrological modelling approaches in a partly glacierized Swiss watershed, Hydrol. Process., 25, 2071–2084, https://doi.org/10.1002/hyp.7958, 2011.

Magnusson, J., Wever, N., Essery, R., Helbig, N., Winstral, A., and Jonas, T.: Evaluating snow models with varying process representations for hydrological applications, Water Resour. Res., 51, 2707–2723, https://doi.org/10.1002/2014WR016498, 2015.

Mankin, J. S., Viviroli, D., Singh, D., Hoekstra, A. Y., and Diffenbaugh, N. S.: The potential for snow to supply human water demand in the present and future, Environ. Res. Lett., 10, 114016, https://doi.org/10.1088/1748-9326/10/11/114016, 2015.

Menard, C. and Essery, R.: ESM-SnowMIP meteorological and evaluation datasets at ten reference sites (in situ and bias corrected reanalysis data), PANGAEA [data set], https://doi.org/10.1594/PANGAEA.897575, 2019.

Ménard, C. B., Essery, R., Barr, A., Bartlett, P., Derry, J., Dumont, M., Fierz, C., Kim, H., Kontu, A., Lejeune, Y., Marks, D., Niwano, M., Raleigh, M., Wang, L., and Wever, N.: Meteorological and evaluation datasets for snow modelling at 10 reference sites: description of in situ and bias-corrected reanalysis data, Earth Syst. Sci. Data, 11, 865–880, https://doi.org/10.5194/essd-11-865-2019, 2019.

Menard, C. B., Essery, R., Krinner, G., Arduini, G., Bartlett, P., Boone, A., Brutel-Vuilmet, C., Burke, E., Cuntz, M., Dai, Y., Decharme, B., Dutra, E., Fang, X., Fierz, C., Gusev, Y., Hagemann, S., Haverd, V., Kim, H., Lafaysse, M., Marke, T., Nasonova, O., Nitta, T., Niwano, M., Pomeroy, J., Schädler, G., Semenov, V. A., Smirnova, T., Strasser, U., Swenson, S., Turkov, D., Wever, N., and Yuan, H.: Scientific and Human Errors in a Snow Model Intercomparison, B. Am. Meteorol. Soc., 102, E61–E79, https://doi.org/10.1175/BAMS-D-19-0329.1, 2021.

Meyer, D., Dimitriadou, E., Hornik, K., Weingessel, A., and Leisch, F.: e1071: Misc Functions of the Department of Statistics, Probability Theory Group (Formerly: E1071), TU Wien, https://cran.r-project.org/package=e1071 (last access: 31 January 2024), 2023.

Mital, U., Dwivedi, D., Özgen-Xian, I., Brown, J. B., and Steefel, C. I.: Modeling Spatial Distribution of Snow Water Equivalent by Combining Meteorological and Satellite Data with Lidar Maps, Artif. Intell. Earth Syst., 1, e220010, https://doi.org/10.1175/AIES-D-22-0010.1, 2022.

Nash, J. E. and Sutcliffe, J. V: River flow forecasting through conceptual models part I – A discussion of principles, J. Hydrol., 10, 282–290, https://doi.org/10.1016/0022-1694(70)90255-6, 1970.

Ohmura, A.: Physical Basis for the Temperature-Based Melt-Index Method, J. Appl. Meteorol., 40, 753–761, https://doi.org/10.1175/1520-0450(2001)040<0753:PBFTTB>2.0.CO;2, 2001.

Oyler, J. W., Dobrowski, S. Z., Ballantyne, A. P., Klene, A. E., and Running, S. W.: Artificial amplification of warming trends across the mountains of the western United States, Geophys. Res. Lett., 42, 153–161, https://doi.org/10.1002/2014GL062803, 2015.

Parajka, J. and Blöschl, G.: The value of MODIS snow cover data in validating and calibrating conceptual hydrologic models, J. Hydrol., 358, 240–258, https://doi.org/10.1016/j.jhydrol.2008.06.006, 2008.

Pepin, N. C., Losleben, M., Hartman, M., and Chowanski, K.: A Comparison of SNOTEL and GHCN/CRU Surface Temperatures with Free-Air Temperatures at High Elevations in the Western United States: Data Compatibility and Trends, J. Climate, 18, 1967–1985, https://doi.org/10.1175/JCLI3375.1, 2005.

R Core Team: R: A language and environment for statistical computing, https://www.r-project.org/ (last access: 31 January 2024), 2020.

Riggs, G., Hall, D., and Salomonson, V.: MODIS snow products user guide to collection 6.1, https://nsidc.org/sites/default/files/c61_modis_snow_user_guide.pdf (last access: 31 January 2024), 2019.

Santi, E., De Gregorio, L., Pettinato, S., Cuozzo, G., Jacob, A., Notarnicola, C., Günther, D., Strasser, U., Cigna, F., Tapete, D., and Paloscia, S.: On the Use of COSMO-SkyMed X-Band SAR for Estimating Snow Water Equivalent in Alpine Areas: A Retrieval Approach Based on Machine Learning and Snow Models, IEEE T. Geosci. Remote, 60, 1–19, https://doi.org/10.1109/TGRS.2022.3191409, 2022.

Scalzitti, J., Strong, C., and Kochanski, A. K.: A 26 year high-resolution dynamical downscaling over the Wasatch Mountains: Synoptic effects on winter precipitation performance, J. Geophys. Res.-Atmos., 121, 3224–3240, https://doi.org/10.1002/2015JD024497, 2016.

Sexstone, G. A., Clow, D. W., Fassnacht, S. R., Liston, G. E., Hiemstra, C. A., Knowles, J. F., and Penn, C. A.: Snow Sublimation in Mountain Environments and Its Sensitivity to Forest Disturbance and Climate Warming, Water Resour. Res., 54, 1191–1211, https://doi.org/10.1002/2017WR021172, 2018.

Shakoor, A., Burri, A., Bavay, M., Ejaz, N., Ghumman, A. R., Comola, F., and Lehning, M.: Hydrological response of two high altitude Swiss catchments to energy balance and temperature index melt schemes, Polar Sci., 17, 1–12, https://doi.org/10.1016/j.polar.2018.06.007, 2018.

Shao, D., Li, H., Wang, J., Hao, X., Che, T., and Ji, W.: Reconstruction of a daily gridded snow water equivalent product for the land region above 45° N based on a ridge regression machine learning approach, Earth Syst. Sci. Data, 14, 795–809, https://doi.org/10.5194/essd-14-795-2022, 2022.

Shwartz-Ziv, R. and Armon, A.: Tabular data: Deep learning is not all you need, Inf. Fusion, 81, 84–90, https://doi.org/10.1016/j.inffus.2021.11.011, 2022.

Sturm, M., Goldstein, M. A., and Parr, C.: Water and life from snow: A trillion dollar science question, Water Resour. Res., 53, 3534–3544, https://doi.org/10.1002/2017WR020840, 2017.

Sun, N., Yan, H., Wigmosta, M. S., Lundquist, J., Dickerson-Lange, S., and Zhou, T.: Forest Canopy Density Effects on Snowpack Across the Climate Gradients of the Western United States Mountain Ranges, Water Resour. Res., 58, e2020WR029194, https://doi.org/10.1029/2020WR029194, 2022.

Terzago, S., Andreoli, V., Arduini, G., Balsamo, G., Campo, L., Cassardo, C., Cremonese, E., Dolia, D., Gabellani, S., von Hardenberg, J., Morra di Cella, U., Palazzi, E., Piazzi, G., Pogliotti, P., and Provenzale, A.: Sensitivity of snow models to the accuracy of meteorological forcings in mountain environments, Hydrol. Earth Syst. Sci., 24, 4061–4090, https://doi.org/10.5194/hess-24-4061-2020, 2020.

Theobald, D. M., Harrison-Atlas, D., Monahan, W. B., and Albano, C. M.: Ecologically-Relevant Maps of Landforms and Physiographic Diversity for Climate Adaptation Planning, PLoS One, 10, 1–17, https://doi.org/10.1371/journal.pone.0143619, 2015.

Tong, R., Parajka, J., Széles, B., Greimeister-Pfeil, I., Vreugdenhil, M., Komma, J., Valent, P., and Blöschl, G.: The value of satellite soil moisture and snow cover data for the transfer of hydrological model parameters to ungauged sites, Hydrol. Earth Syst. Sci., 26, 1779–1799, https://doi.org/10.5194/hess-26-1779-2022, 2022.

Umirbekov, A., Essery, R., and Müller, D.: GEMS: Generalizable empirical model of snow accumulation and melt (version 1.0), Zenodo [code], https://doi.org/10.5281/zenodo.10161423, 2023.

USDA: Chapter 6 Data Management, in: Part 622 Snow Survey and Water Supply Forecasting, National Engineering Handbook, Natural Resources Conservation Service, USDA, https://directives.sc.egov.usda.gov/35529.wba (last access: 31 January 2024), 2014.

USDA: Air & Water Database Report Generator v2.0, https://wcc.sc.egov.usda.gov/reportGenerator/ (last access: 31 January 2024), 2016.

USDA: SNOTEL Historical Air Temperature Bias Correction Metadata, https://www.nrcs.usda.gov/resources/guides-and-instructions/air-temperature-bias-correction (last access: 29 January 2024), 2019.

Vafakhah, M., Nasiri Khiavi, A., Janizadeh, S., and Ganjkhanlo, H.: Evaluating different machine learning algorithms for snow

water equivalent prediction, Earth Sci. Inf., 15, 2431–2445, https://doi.org/10.1007/s12145-022-00846-z, 2022.

Vapnik, V. N.: The Nature of Statistical Learning, I., Springer, New York, NY, USA, 224 pp., https://doi.org/10.1007/978-1-4757-2440-0, 1995.

Vert, J. P., Tsuda, K., and Schölkopf, B.: A Primer on Kernel Methods, in: Kernel Methods in Computational Biology, MIT Press, Cambridge, MA, USA, 35–70, https://doi.org/10.7551/mitpress/4057.003.0004, 2004.

Wang, Y.-H., Gupta, H. V., Zeng, X., and Niu, G.-Y.: Exploring the Potential of Long Short-Term Memory Networks for Improving Understanding of Continental- and Regional-Scale Snowpack Dynamics, Water Resour. Res., 58, e2021WR031033, https://doi.org/10.1029/2021WR031033, 2022.

Wickham, H., François, R., Henry, L., Müller, K., and Vaughan, D.: dplyr: A Grammar of Data Manipulation, https://cran.r-project.org/package=dplyr, 2023.

Zambrano-Bigiarini, M.: hydroGOF: Goodness-of-fit functions for comparison of simulated and observed hydrological time series, Zenodo [code], https://doi.org/10.5281/zenodo.839854, 2020.

Zhang, T.: Influence of the seasonal snow cover on the ground thermal regime: An overview, Rev. Geophys., 43, https://doi.org/10.1029/2004RG000157, 2005.